EFFECT OF TEMPERATURE ON VISIBLE PHOTOLUMINESCENCE OF THERMALLY ANNEALED PbSe NANOCRYSTALLINE FILMS

Wei Wu, Bo Li, Xia Xiang*, Xiaotao Zu

School of Physics, University of Electronic Science and Technology of China, Chengdu, China; e-mail: xiaxiang@uestc.edu.cn

The photoluminescence (PL) performance of thermally annealed PbSe nanocrystalline films has been investigated at different temperatures. The visible PL signals at 655 and 466 nm are observed for the as-prepared PbSe films, and the enhanced intensities of the two PL peaks are closely related to the optimized crystallization quality of PbSe nanoparticles after annealing at 50–150°C. However, as the annealing temperature is above 200°C, the severe surface damage of PbSe films induced by the oxide impurity phases and dislocation defects results in the reduction of the crystallinity of PbSe and the lower intensities of PL signals, which have been proved by means of X-ray diffraction (XRD) characterization. In addition, another emission peak at 429 nm is observed at the annealing temperature above 200°C owing to the appearance of the PbO impurity phase, and its intensity strongly depends on the content of the PbO impurity phase, whereas the PL intensity decreases above 350°C owing to the formation of $PbSeO_x$.

Keywords: *PbSe film, annealing temperature, photoluminescence, PbO impurity phase, dislocation density.*

ВЛИЯНИЕ ТЕМПЕРАТУРЫ НА ВИДИМУЮ ФОТОЛЮМИНЕСЦЕНЦИЮ ТЕРМИЧЕСКИ ОТОЖЖЕННЫХ НАНОКРИСТАЛЛИЧЕСКИХ ПЛЕНОК PbSe

W. Wu, B. Li, X. Xiang*, X. Zu

УДК 535.37:539.216.2

Школа физики Китайского университета электронной науки и технологии, Чэнду, Китай; e-mail: xiaxiang@uestc.edu.cn

(Поступила 9 февраля 2022)

Исследована фотолюминесценция (ФЛ) нанокристаллических пленок PbSe, отожженных при различных температурах. Видимая ФЛ на длинах волн 655 и 466 нм наблюдается для свежеприготовленных пленок PbSe, а повышенная интенсивность двух максимумов ФЛ связана с оптимизированным качеством кристаллизации наночастиц PbSe после отжига при 50–150°C. Поскольку температура отжига >200°C, сильное повреждение поверхности пленок PbSe, вызванное примесными фазами оксида и дефектами дислокаций, приводит к снижению кристалличности PbSe и более низким интенсивностям ФЛ, что подтверждено методом рентгеновской дифракции. При температуре отжига >200°C наблюдается еще один максимум излучения при 429 нм из-за появления примесной фазы PbO, интенсивность которого сильно зависит от содержания PbO, тогда как при температуре >350°C интенсивность ФЛ уменьшается из-за образования $PbSeO_x$.

Ключевые слова: *пленка PbSe, температура отжига, фотолюминесценция, примесная фаза PbO, плотность дислокаций.*

Introduction. Lead chalcogenides, a class of IV–VI semiconductor materials with narrow band gaps, are very popular in the application of functional devices such as light-emitting diodes [1], laser diodes [2], infrared detectors [3], solar cells [4], thermoelectric devices [5], photosensors [6], etc., owing to their excellent physical properties. Among the lead chalcogenide materials, lead selenide (PbSe) has a large exciton Bohr radius (46 nm), a small effective mass of the excited electron-hole pair, and high carrier mobility, which leads to the remarkable quantum confinement effect in large crystals [7–9] and thus attracts much at-

tention in the field of solar cells. In recent years, PbSe nanocrystalline films have been studied in an endless stream because of their band gap tunability and good photoluminescence (PL) performance, etc. For example, Feng et al. found that the optical band gap of PbSe films varied from 2.02 to 1.26 eV with the increasing grain size [10]. The study by Hone and Dejene revealed that the intensity of the PL emission peak increased with the thickness of PbSe films [11]. It can be seen that these properties are largely affected by a microstructure of PbSe films, which depends to a great extent on experimental procedures and corresponding parameters.

Post-processing, such as thermal annealing, holds the advantages of improving or modifying the physical properties of PbSe films by optimizing the microstructure or incorporating particular elements [12–15]. The sensitization process of thermal annealing in oxygen or iodine atmosphere has attracted extensive attention in the past decades because it can effectively improve the infrared detection performance of PbSe films [16–22]. Kumar et al. conducted the annealing treatment of poly-crystalline PbSe films in oxygen and iodine-rich atmospheres to obtain the PbSe photoconductor with high performance and they also investigated the crystal structure, phase formation, and chemical analysis of the unknown phases to understand the photoconductive mechanisms [23]. In addition, the thermally annealed PbSe films in the oxygen atmosphere showed greatly enhanced PL signals in the infrared region by an increase of two orders of magnitude in the PL intensity at 4.5 μm owing to surface passivation of PbSe films [24]. Ma et al. prepared PbSe films with a grain size of 5 nm in silicate glass by a double-stage annealing procedure and the strongest PL peak was observed at 1575 nm, indicating the potential application of PbSe films in optical fiber communication [25]. However, the visible photoluminescence performance of PbSe films with annealing treatment in an inert gas atmosphere has not been widely studied.

We have discussed the influence of sputtering power and deposition time on the intensity of the PL emission peak at 655 nm, which correlates quite well with crystallization quality and morphology of PbSe films [26]. Based on the previous work, thermal annealing in the Ar gas atmosphere was conducted to obtain PbSe films with better visible PL performance in this work. The intensity variation of the two PL peaks at 655 and 466 nm is consistent with the changed crystallinity of annealed PbSe films. The PL signal at a shorter wavelength (429 nm) appears after annealing at 200°C, and its intensity is strongly dependent on the content of the PbO impurity phase.

Experiment details. PbSe nanocrystalline films were deposited on the cleaned waterjet-cut quartz glass from a PbSe target (99.999% purity) by the magnetron sputtering method. The sputtering process was carried out in the Ar atmosphere with a pressure of 1.5 Pa, and the sputtering power and deposition time were set at 120 W and 30 min respectively. The prepared PbSe films were put into a tube furnace for annealing in the flowing Ar atmosphere with a flux of 300 mL/min. The samples were annealed for 1 h at different temperatures from 50 to 400°C by an increment of 50°C, with a heating rate of 5°C/min.

The photoluminescence spectra were obtained by a Shimadzu spectrofluorophotometer (RF-5301). The crystalline structures were characterized by a Bruker AXS D8 ADVANCE X-ray diffractometer (XRD) with a CuK_α (λ = 1.5418 Å, 40 kV, 40 mA) radiation source. The element compositions and electronic states were analyzed using an X-ray photoelectron spectroscope (XPS, Quantum 2000 Scanning ESCA Microprobe instrument).

The crystallization quality of PbSe films was evaluated by estimating the structural parameters. Based on the results of XRD, the crystallinity and microstrain of PbSe films were calculated using the area under the curve method [27] and the following equation [28]:

$$\varepsilon = (\beta\cos\theta)/4,$$

where ε is the microstrain, β is the full width at half the maximum of the diffraction peak, and θ is the diffraction angle corresponding to the diffraction peak. The dislocation density δ is defined using Williamson and Smallman's formula [29],

$$\delta = 1/D^2,$$

where D is the average grain size, which is calculated using Scherrer's equation [30].

Results and discussion. Photoluminescence is a key factor in evaluating the performance of luminescent materials for applications. Generally, the PL signal is caused by the recombination of excited electrons and holes not only from the high-quality surface but also from the defects or impurities, which will provide new states for materials. PL spectra usually reflect the information on the microstructure such as crystallinity, impurity, defect, etc. [31]. Based on our previous study [26], an excitation radiation source with a wave-

length of 404 nm was selected to measure the PL emission spectra of PbSe films, and the results are shown in Fig. 1. Two PL signals located at around 466 and 655 nm were detected within the visible range for the as-prepared PbSe films, which may be attributed to the interstitial atom or vacancy defects [32]. The intensity of the emission peak at 655 nm shows a nonmonotonic change with the increasing annealing temperature, and similar variation is observed for the emission peak at 466 nm, as shown in Fig. 1a and c. The third PL signal in the violet region probably originated from PbO and is observed at 429 nm for PbSe films annealed at a temperature above 200°C, as shown in Fig. 1d, which will be confirmed by the subsequent XRD and XPS results. The variation in PL spectra indicates a complex evolution in the microstructure of thermally annealed PbSe films. Therefore, the crystalline structures of PbSe films were first analyzed by the XRD characterization.

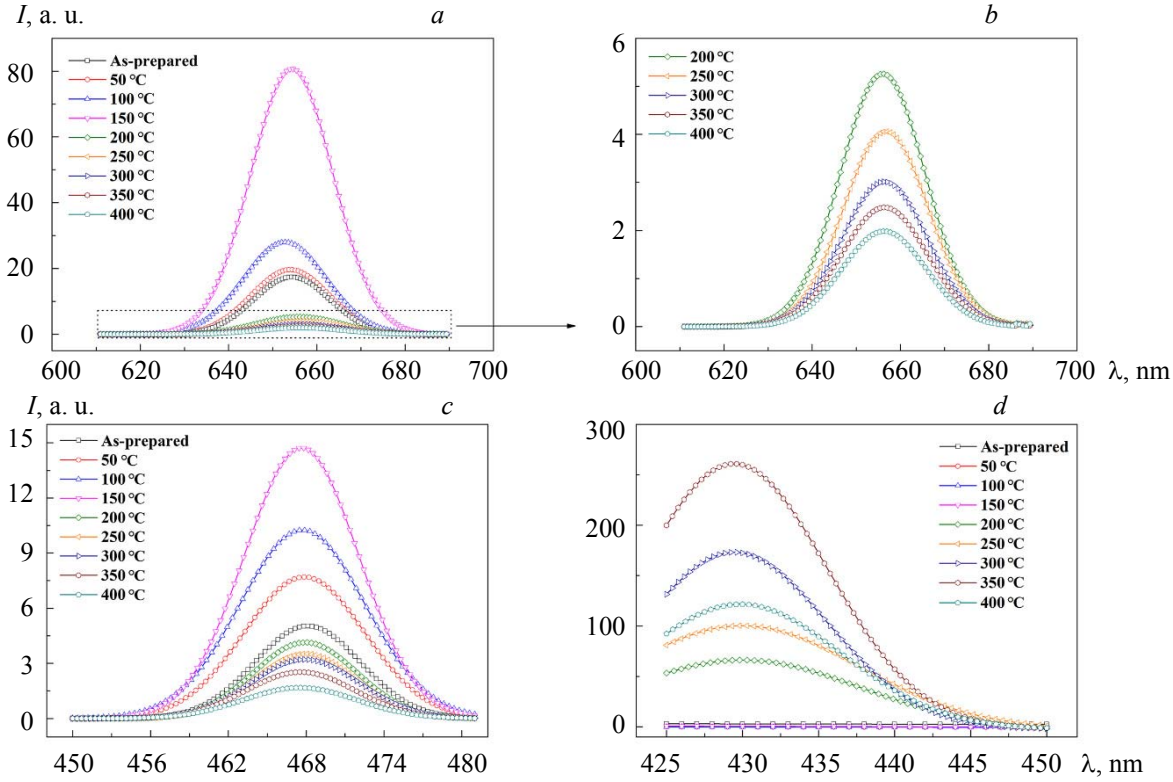

Fig. 1. PL emission spectra at (a) 655, (c) 466, and (d) 429 nm of as-prepared and thermally annealed PbSe films; (b) magnified view of PL emission spectra at 655 nm of PbSe films annealed at 200–400°C.

Figure 2a shows the changes in the intensities of PL peaks at 655 and 466 nm and calculated crystallinity with the increasing annealing temperature. The crystallization quality was improved at the annealing temperatures below 150°C, which is consistent with the enhancement of PL emission peaks at 655 and 466 nm. The lattice structure obeys the cubic system in accordance with JCPDS standard card (NO. 78-1903), where the diffraction peaks at 25.2, 29.1, 41.6, 49.3, 51.5, 60.3, 68.6, and 76.1° correspond to (111), (200), (220), (311), (222), (400), (420), and (442) planes respectively, as shown in Fig. 2b. As for PbSe films annealed above 200°C, the diffraction peaks of oxides (PbO, SeO_2, $PbSeO_3$, and $PbSeO_4$) [22, 33] appear and gradually strengthen with the increasing annealing temperature, and even replace the diffraction peak of PbSe at 29.1°. This could be associated with the lower dissociation energy of Pb-Se (302 kJ/mol) compared with Pb-O (382 kJ/mol) and Se-O (464 kJ/mol), which facilitates the formation of several oxides [34]. Moreover, the Se atoms partly evaporate owing to its lower melting point during annealing at higher temperature, resulting in the existence of lead impurities, which combine with the adsorbed O atoms to form lead oxides after PbSe films are exposed to air. As the PL signal at 429 nm may be related to the PbO impurity phase, and the diffraction peak of PbO is not obvious at 250°C, the content of the PbO impurity phase was analyzed in detail below. Figure 2c demonstrates the change of calculated dislocation density of the PbSe film with the annealing temperature. The dislocation density decreases with the increase in the annealing temperature from 50 to

200°C, which results from the optimization of the PbSe film. However, the dislocation density increases again at annealing temperature above 200°C because of the formation of oxide impurity phases, i.e., PbO, SeO_2, $PbSeO_3$, and $PbSeO_4$. The resultant impurity phases and dislocation defects on the surface of PbSe films seriously damage the crystalline structure and introduce the trapping mechanism of photogenerated carriers, and eventually lead to the significant reduction in intensities of PL peaks at 655 and 466 nm. On the other hand, the main diffraction peak of PbSe turns from (200) to (220), and then to (111) at the temperature from 150 to 400°C, which could be related to the change of microstrain. Figure 2d shows that the total microstrain of PbSe films decreases with the increase of the annealing temperature, indicating that the variation of dominated growth direction of PbSe films tends to minimize the strain energy of the system, which is consistent with our previous work [26].

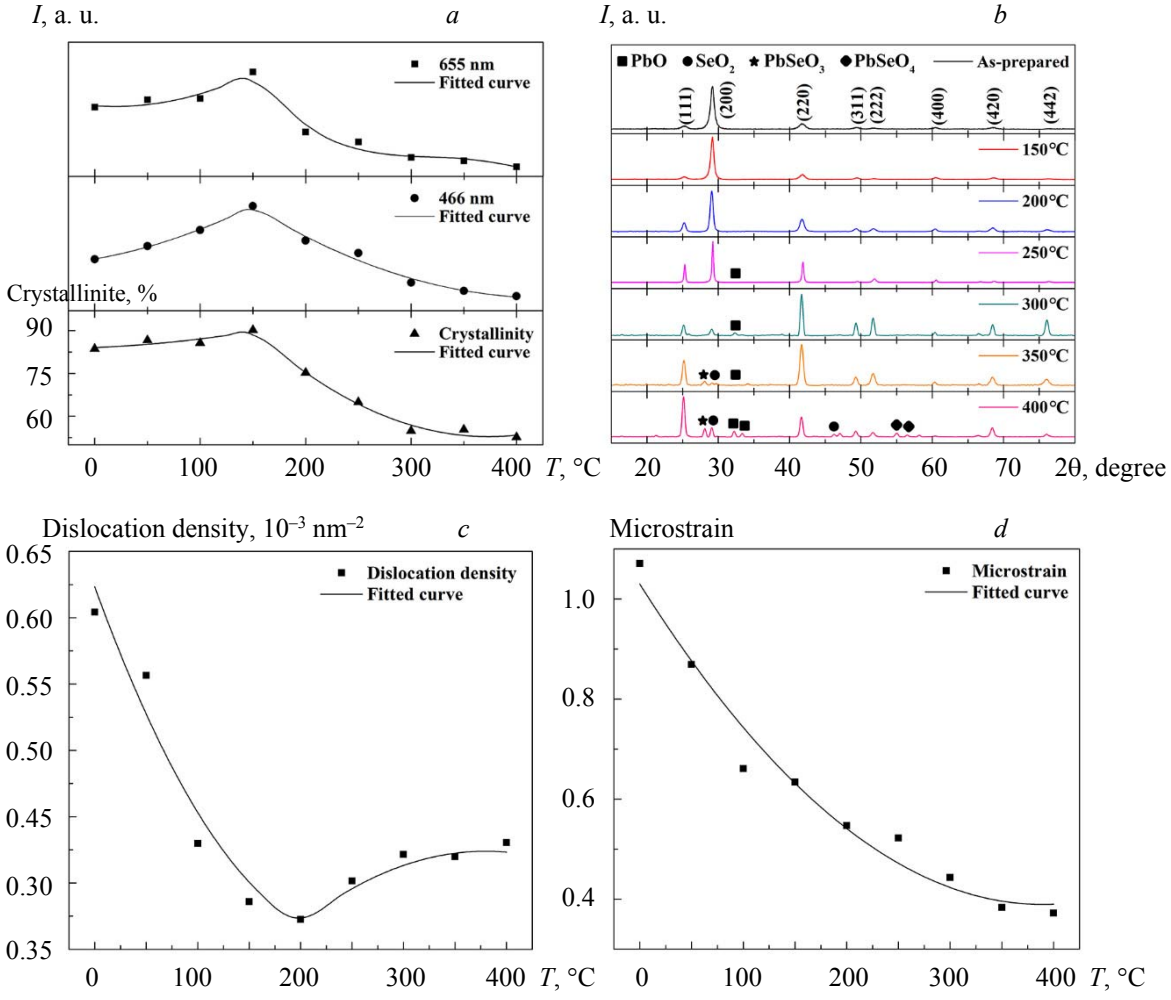

Fig. 2. (a) Variation of crystallinity and PL intensity changes at 655 and 466 nm at different temperatures; (b) XRD patterns of PbSe films annealed at 150–400 °C; variations of (c) dislocation density and (d) total microstrain at different annealing temperatures.

The XPS characterization is often used to reveal the surface chemical state of nanomaterials [35]. The peaks at 137.6 and 142.6 eV are related to Pb $4f_{7/2}$ and Pb $4f_{5/2}$, respectively, as shown in Fig. 3a. Both can be divided into two Gaussian peaks. The peaks at 137.3 and 142.0 eV come from PbSe, whereas the other two, 138.3 and 143.3 eV, are attributed to PbO [36]. The fitting results of the Se 3d state are given in Fig. 3b. The peak at lower binding energy of 53.4 eV is assigned to PbSe, which can be fitted with two peaks associated with Se $3d_{5/2}$ and Se $3d_{3/2}$, respectively. The peak ascribed to SeO_2 is located at a higher binding energy of 58.5 eV, consistent with Sun et al. [36]. The results verify the presence of oxides on the surface of PbSe

films. Furthermore, the content variations of Pb, Se, and O atoms are calculated using the quantitative relative sensitivity factors method [26]. As shown in Fig. 3c and d, the relationship between the Pb/Se atomic ratio and annealing temperature shows a gradually increasing trend, indicating the deficiency of the Se atomic content, whereas the relative content variation of PbO/PbSe shows a similar trend. The result confirms the increase in the PbO impurity phase content, which is highly consistent with the XRD results.

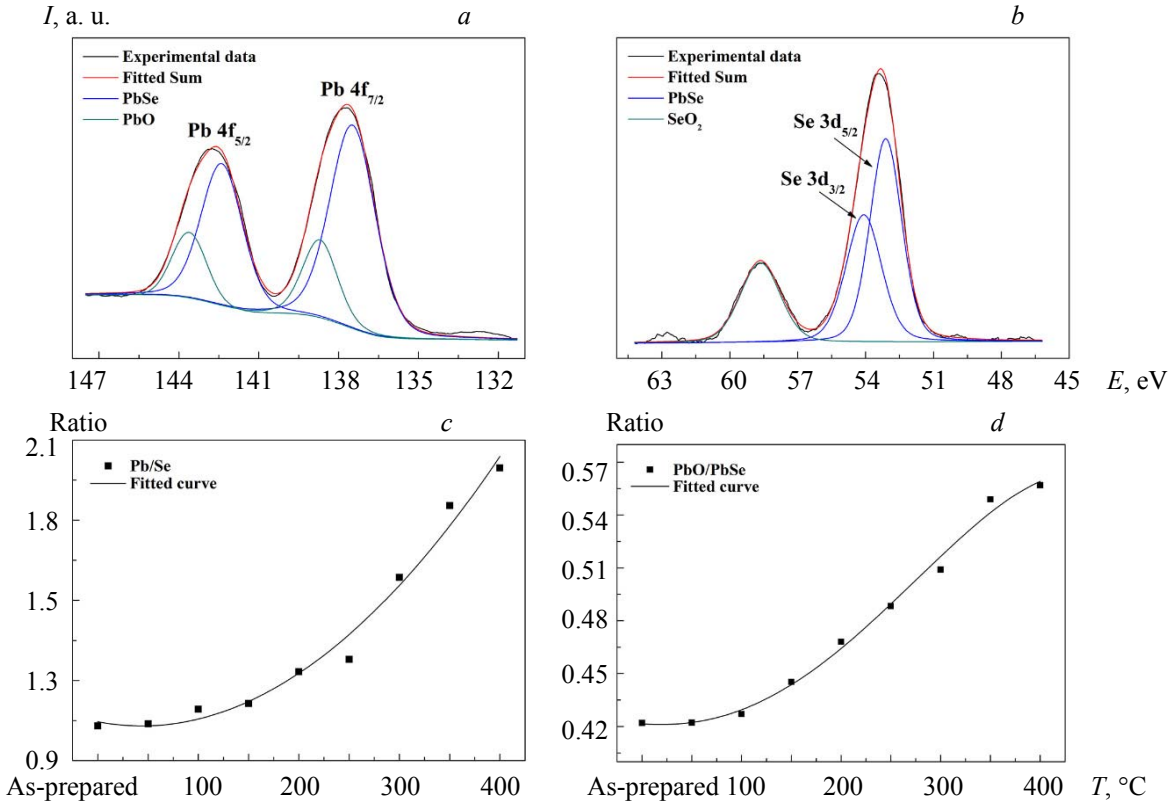

Fig. 3. XPS fitting curves of (a) Pb 4*f* and (b) Se 3*d*; variations of (c) Pb/Se atomic ratio and (d) relative content of PbO/PbSe at different annealing temperatures.

As mentioned above, the PL peak at 429 nm is related to the content of the PbO impurity phase. A similar emission peak at 440 nm was reported for PbO nanoparticles synthesized by the chemical precipitation method [32]. Therefore, the PbO impurity phase should contribute to the PL signal at 429 nm in this work. As shown in Fig. 4a, the PL intensity increases at 200–350°C, which is in accordance with the increasing content of the PbO impurity phase (Fig. 3d). Nevertheless, a drop in the PL intensity occurs as the annealing temperature reaches 400 °C. This could be associated with the formation of the $PbSeO_x$ (x = 3 or 4) phase on the PbSe film surface, and the corresponding diffraction peaks in the XRD patterns are obviously enhanced at 400°C. The formation of the $PbSeO_x$ phase is possibly relevant to the inevitable adsorption of oxygen atoms on the film surface before annealing treatment, and the following reactions tend to occur at a relatively high temperature [37]:

$$PbSe^{solid} + 1.5O_2^{gas} \rightarrow PbSeO_3^{solid} \quad (1)$$

$$PbSe^{solid} + 2O_2^{gas} \rightarrow PbSeO_4^{solid} \quad (2)$$

$$PbSeO_3^{solid} + 0.5O_2^{gas} \rightarrow PbSeO_4^{solid} \quad (3)$$

$$PbO^{solid} + SeO_2 \rightarrow PbSeO_3^{solid} \quad (4)$$

The intensity of the PL peak at 429 nm does not decrease significantly at an annealing temperature of 350°C, which may be relevant to the lower content of the $PbSeO_x$ phase compared with the PbO phase. The content of the $PbSeO_x$ phase increases owing to the reactions (1)–(4) when the annealing temperature is 400°C, which prevents further formation of the PbO phase and leads to the decrease in the PL intensity.

Figure 4b shows the schematic diagrams of oxide impurities formation on the surface of PbSe films before and after thermal annealing at 400 °C. The adsorbed oxygen atoms on the surface combine with Pb and Se atoms so that a small amount of PbO and SeO_2 formed before annealing. After annealing at 400°C, $PbSeO_x$ appears on the film surface, which results in the decrease in the PL intensity at 429 nm related to PbO.

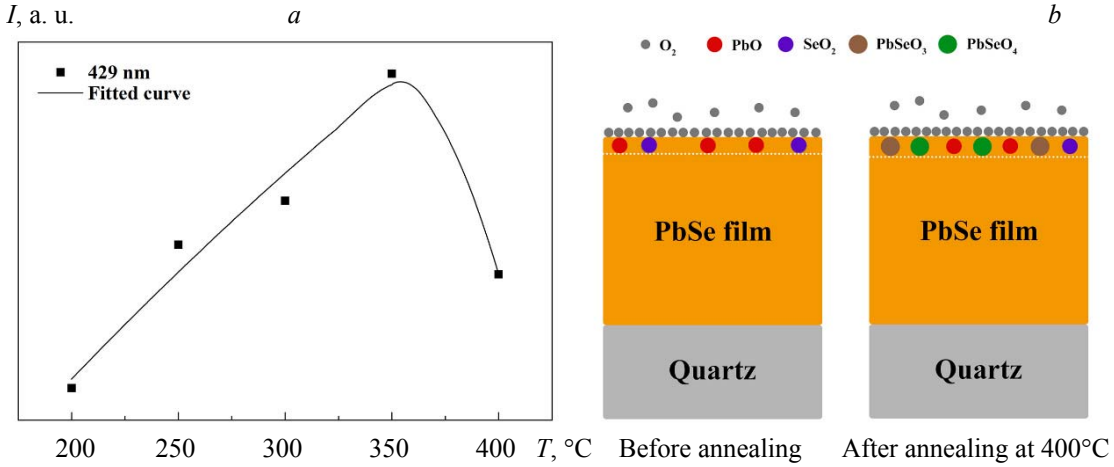

Fig. 4. (a) Intensity variation of the PL peak at 429 nm at different annealing temperatures; (b) schematic diagrams of PbSe films before and after thermal annealing at 400°C.

Conclusions. PbSe nanocrystalline films prepared by magnetron sputtering technology were thermally annealed at temperatures of 50–400°C. PL intensities at 655 and 466 nm strengthened because of the improved crystallization quality after annealing at temperatures below 150°C. However, the crystallinity of PbSe films reduced after annealing at higher temperatures because the impurity phases and dislocation defects were introduced into the films, which led to the decrease in the PL intensity. The emission peak at 429 nm responsible for PbO appeared and its intensity became higher with the increase in the annealing temperature from 200 to 350°C. Nevertheless, the PL intensity at 429 nm dropped after annealing at 400°C because of the formation of $PbSeO_x$.

Acknowledgements. This work was supported by the National Natural Science Foundation of China-China Academy of Engineering Physics Joint Foundation (NSAF) of China (Grant U1630126).

REFERENCES

1. A. Namekawa, R. Katoh, *Chem. Phys. Lett*., **659**, 154–158 (2016).
2. V. Arivazhagan, M. M. Parvathi, S. Rajesh, *Vacuum*, **99**, 95–98 (2014).
3. L. Zhang, Y. Zhang, S. V. Kershaw, et al., *Nanotechnology*, **25**, 105704 (2014).
4. T. Tohidi, K. Jamshidi-Ghaleh, *Appl. Phys. A*, **118**, 1247–1258 (2015).
5. J. P. Heremans, V. Jovovic, E. S. Toberer, et al., *Science*, **321**, 554–557 (2008).
6. H. Zogg, S. Blunier, T. Hoshino, et al., *IEEE Trans Electron Devices*, **38**, 1110–1117 (1991).
7. F. W. Wise, *Acc. Chem. Res*., **33**, 773–780 (2000).
8. W. L. Ma, J. M. Luther, H. M. Zheng, et al., *Nano Lett*., **9**, 1699–1703 (2009).
9. Y. Liu, M. Gibbs, J. Puthussery, et al., *Nano Lett*., **10**, 1960–1969 (2010).
10. W. R. Feng, X. Y. Wang, H. Zhou, et al., *Vacuum*, **109**, 108–111 (2014).
11. F. G. Hone, F. B. Dejene, *J. Mater. Sci. Mater. Electron*., **28**, 5979–5989 (2017).
12. M. Bouroushian, Z. Loizos, N. Spyrellis, et al., *Thin Solid Films*, **229**, 101–106 (1993).
13. L. M. Peter, R. L. Wang, *Electrochem. Commun*., **1**, 554–558 (1999).
14. S. P. Zimin, I. I. Amirov, V. V. Naumov, *Semiconductors*, **50**, 1125–1129 (2016).
15. R. P. Sugavaneshwar, T. D. Dao, T. Yokoyama, et al., *Radiation Effects and Defects in Solids*, **173**, 112–117 (2018).
16. L. P. Biro, R. M. Candea, G. Borodi, et al., *Thin Solid Films*, **165**, 303–315 (1988).
17. M. C. Torquemada, M. T. Rodrigo, G. Vergara, et al., *J. Appl. Phys*., **93**, 1778–1784 (2003).

18. V. Kasiyan, Z. Dashevsky, C. M. Schwarz, et al., *J. Appl. Phys*., **112**, 086101 (2012).
19. P. Kumar, M. Pfeffer, E. Schweda, et al., *J. Alloys Compd*., **724**, 316–326 (2017).
20. S. Ganguly, S. Yoo, *J. Electron. Mater*., **48**, 6169–6175 (2019).
21. L. N. Maskaeva, V. M. Yurk, V. F. Markov, et al., *Semiconductors*, **54**, 1191–1197 (2020).
22. S. Y. Yan, Q. Yang, S. L. Feng, et al., *J. Electron. Mater*., **49**, 4929–4935 (2020).
23. P. Kumar, M. Pfeffer, C. Berthold, et al., *J. Alloys Compd*., **735**, 1654–1661 (2018).
24. F. Zhao, S. Mukherjee, J. Ma, et al., *Appl. Phys. Lett*., **92**, 211110 (2008).
25. D. W. Ma, C. Cheng, Y. N. Zhang, et al., *Opt. Mater*., **37**, 834–839 (2014).
26. W. Wu, Y. L. Tang, B. Li, et al., *Opt. Mater*., **118**, 111233 (2021).
27. W. E. Mahmoud, *Polym. Adv. Technol*., **22**, 2550–2555 (2011).
28. M. R. A. Bhuiyan, M. A. A. Azad, S. M. F. Hasan, *Indian J. Pure. Appl. Phys*., **49**, 180–185 (2011).
29. G. K. Williamson, R. E. Smallman, *Philos. Mag*., **1**, 34–46 (1956).
30. J. I. Langford, A. J. C. Wilson, *J. Appl. Cryst*., **11**, 102–113 (1978).
31. T. H. Gfroerer, In: Encyclopedia of Analytical Chemistry, John Wiley & Sons, Ltd. (2006), https://doi.org/10.1002/9780470027318.a2510
32. N. Mythili, K. T. Arulmozhi, *Int. J. Sci. Eng. Res*., **5**, 412–416 (2014).
33. R. Yousefi, A. K. Zak, F. Jamali-Sheini, et al., *Ceram. Int*., **40**, 11699–11703 (2014).
34. C. Gautier, M. Cambon-Muller, M. Averous, *Appl. Surf. Sci*., **141**, 157–163 (1999).
35. C. Cai, S. B. Han, X. T. Zhang, et al., *RSC Adv*., **12**, 6205–6213 (2022).
36. X. G. Sun, K. W. Gao, X. L. Pang, et al., *Appl. Surf. Sci*., **356**, 978–985 (2015).
37. V. V. Tomaev, L. L. Makarov, P. A. Tikhonov, et al., *Glass Phys. Chem*., **30**, 349–355 (2004).